RESEARCH

Open Access

Synergetic Influence of Microcrystalline Quartz and Alkali Content in Aggregate on Deterioration of Concrete Railroad Ties Used for 15 Years in High-Speed Railways

Dongho Jeon[1,2], Juan Yu[1,2], Jihwan Kim[1,2], Seyoon Yoon[1,2], Younghoon Bae[1*] and Jae Eun Oh[2*]

Abstract

This study investigated the deteriorations of precast prestressed concrete (PSC) ties that were used for 15 years in high-speed railways in Korea and its damaging mechanism. The collected PSC ties with longitudinal cracks on sides and map cracks on surfaces exhibited strength degradation. The deteriorations were likely related to alkali-silica reaction (ASR) and delayed ettringite formation (DEF) together, given that the presence of massive ettringite crystals and the decomposition of ASR gel were found from microstructural analyses. Although there were no typical reactive siliceous aggregates for ASR in this study, ASR cracks were generated in the PSC ties. This is because the aggregates in the PSC ties with cracks were potentially reactive, and its high alkali-silica reactivity was likely attributable to the presence of microcrystalline quartz, supplying reactive SiO_2 to trigger ASR. Furthermore, the alkali content in aggregates was associated with the deterioration of the PSC ties. The alkali-bearing minerals in aggregates (i.e., alkali feldspars) likely supplied enough alkalis for ASR. Besides, micas in aggregates could promote ASR due to their porous structure, which helps easy water ingress.

Keywords: alkali-silica reaction, delayed ettringite formation, concrete railroad tie, alkali-bearing minerals, microcrystalline quartz

1 Introduction

In the infrastructural railroad system, precast prestressed concrete (PSC) has been mainly used for manufacturing concrete railroad ties and track slabs (Ma et al., 2017). PSC products are generally manufactured by steam curing to accelerate strength development and increase concrete production efficiency with fast mold release (Ho et al., 2003; Jeong et al., 2015). However, signs of deterioration, such as surface peelings or surface cracks in steam-cured concrete, have been reported (Hime, 1996; Sahu & Thaulow, 2004). The cases were mainly due to internal sulfate attack, also known as delayed ettringite formation (DEF), which causes cracking of concrete. DEF has often been observed in steam-cured concretes when steam curing exceeds approximately 65 °C. During stream curing, a high temperature over 65 °C destabilizes ettringite in concrete and releases sulfate ions into the cementitious matrix; after extended use in service at ambient temperature, the released sulfate ions form ettringite in concrete and cause extensive cracking (Monteiro, 2006; Sahu & Thaulow, 2004).

For the failure of PSC ties in railroads, many investigations have been conducted by focusing on estimating the

Jeon *et al. Int J Concr Struct Mater*   (2022) 16:57

Page 2 of 15

residual life of PSC ties by measuring flexural strength and degree of degradation (Remennikov & Kaewunruen, 2014; Thun et al., 2008; Bae et al., 2018). Remennikov et al. (Remennikov & Kaewunruen, 2014) collected concrete ties, which were used for 30 years in Australia, and conducted surface abrasion tests, compressive strength tests on cored samples, flexural strength tests, and impact loading tests to ensure that the collected ties could still be used. Thun et al. (Thun et al., 2008) reported that although there was a relationship between the degradation degree of cracked concrete ties and the failure loads in the static flexural strength test, fatigue resistance was barely related to the degree of cracks. Bae et al. (2018) studied crack propagation mechanisms and crack-width change by applying fatigue load to cracked ties.

In the Republic of Korea (Korea), PSC has been used for manufacturing concrete railroad ties since 1958 to replace wooden ties, which were less durable and weaker than concrete ties (H F W Taylor et al., 2001). Railroad ties directly support train load and transfer the load to the track ballast and ground; thus, the durability of railroad ties has been a critical issue due to concerns over the safe and economic operation of the railroad system (Kaewunruen & Remennikov, 2006). In particular, in 2004, with the opening of the Gyeongbu High-Speed Railway (HSR) (at a maximum train speed of 300 km/h), which was the first high-speed railroad in Korea, the durability of PSC ties has become more critical as it should resist heavy and high-speed impact loads of passing trains. However, many PSC ties in the Gyeongbu HSR have been replaced due to notable cracks and surface deterioration, which significantly formed before the end of their expected service life of 40 years (Railways 2004). Interestingly, although the concrete ties were made in the same manufacturing factory using the same concrete mixture proportion and curing condition, different types of degradations were developed among the ties during the same service period. This phenomenon prompted the necessity for a comprehensive study on the deterioration of concrete ties of the Gyeongbu HSR; however, earlier studies in Korea have simply examined the mechanical aspects of degraded concrete ties and barely conducted microstructural and chemical examinations, which are necessary to understand the underlying deterioration mechanisms of cracked concrete ties (Koh & Hwang, 2015).

This study demonstrates a series of observations of the 15-year used dismantled PSC ties in the Gyeongbu HSR in Korea, which were severely damaged by alkali-silica reaction (ASR) and DEF. However, the deterioration did not result from the well-known conditions associated with generating ASR, but a result of rare causes. The causes were characterized by conducting a static flexural loading test, optical microscopy, powder X-ray diffraction, thermogravimetry, inductively coupled plasma-optical emission spectroscopy, alkalinity measurement, polarization microscope analysis, and scanning electron microscopy with energy dispersive spectroscopy.

2 Experimental

2.1 Field Investigation and Sampling

A total of 441 dismantled PSC ties were collected from the ballasted track of the Gyeongbu HSR in Korea, which is located $183.195 - 183.460$ km from Seoul Station, as shown in Fig. 1a. Fig. 1b–d shows the photographs taken during the field investigation to collect the sample ties in 2019.

All collected PSC ties were manufactured by Taemyung Industrial Co., Ltd., South Korea; a high-strength concrete of 60 MPa (28 days) for the ties was made of Type III Portland cement without adding any supplementary cementitious materials (e.g., no fly ash), and prestressing steel wires of 1705 MPa (yield) were used. The PSC ties were installed in the Gyeongbu HSR in 2002 and were used for field testing for 2 years during the trial run of HSR from 2002 to 2004; after then, the ties had been used in service for 15 years from 2004 to 2018.

After visual inspection, the collected ties were classified into three groups: (1) ties without visible cracks (denoted Non-cracked); (2) ties with horizontally large cracks on sides (denoted Longitudinal-cracked), and (3) ties with reticular cracks (or map cracks) on surfaces (denoted Map-cracked). As control samples for comparison, three Brand-new PSC ties (denoted Brand-new) were obtained; they were manufactured in 2018, but never used. Photographs and details for these PSC ties are summarized in Fig. 2 and Table 1. The Brand-new PSC ties showed very smooth and clean surfaces without any cracks. The Non-cracked PSC ties showed a few minor cracks and rough textures on the surfaces, which were likely due to the long-term outdoor exposure and abrasion by ballast gravels. The Longitudinal-cracked PSC ties noticeably exhibited visibly wide longitudinal cracks (average crack widths $= \sim 5$–6 mm). Lastly, the Map-cracked PSC ties showed reticular cracks, spalling of concrete, and exposure of coarse aggregates.

Among the dismantled 441 PSC ties, 211 ties (47.8%) were classified as Non-cracked, while 228 ties (51.7%) were categorized as Longitudinal-cracked and only two ties were identified as Map-cracked.

2.2 Static Flexural Loading Test

Static flexural loading tests were conducted on rail seat sections, as shown in Fig. 3, in accordance with the European Standards (EN) ((CEN) 2009), for all collected PSC ties and Brand-new ties. The distance between the loading point and each end support was 300 mm, and the
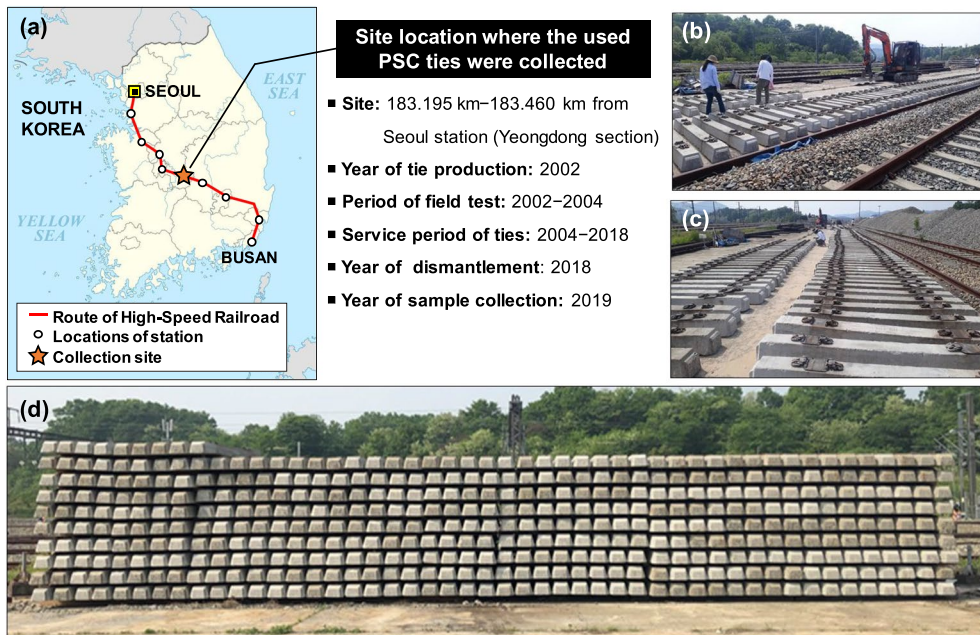
Fig. 1 Information on the collection site and collected dismantled ties: **a** the route of Gyeongbu HSR, **b**–**d** photographs of collection sites and 441 collected PSC ties.
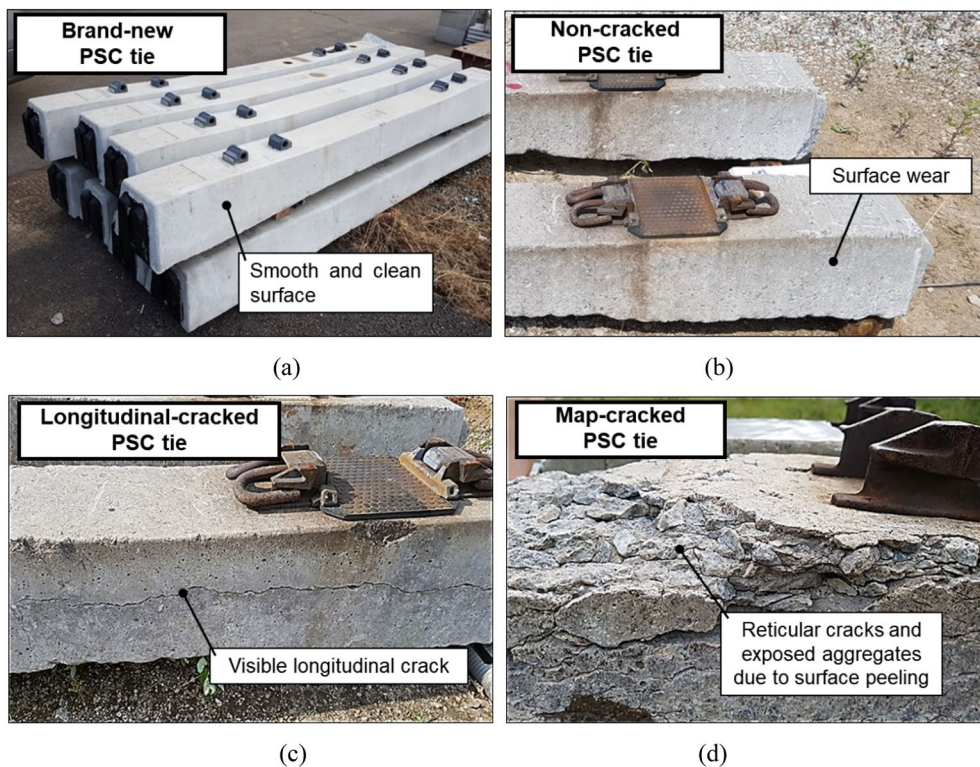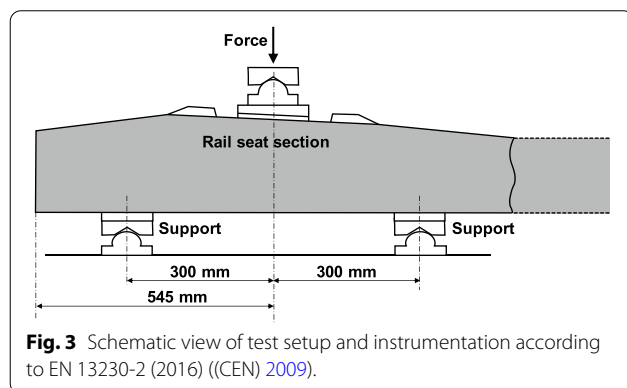

Fig. 2 Photographs of PSC ties: **a** Brand-new, **b** Non-cracked, **c** Longitudinal-cracked, and **d** Map-cracked.

Jeon *et al. Int J Concr Struct Mater*   (2022) 16:57

Page 4 of 15

Table 1 Summary of the collected 441 PSC ties and the brand-new 3 PSC ties for the static flexural loading test and microstructural analyses.

Sample label	Year of production (service life)	Number of samples	Results of visual inspection
Brand-new	2018 (unused)	3	- No crack on surfaces
			- Clear and smooth surfaces
441 PSC ties			
Non-cracked	2002 (15 years)	211	- Slight surface abrasion
Longitudinal-cracked			- Generally good condition
		228	- Long and severe longitudinal cracks on sides
			- Some surface peelings
Map-cracked		2	- Reticular cracks (or map cracks)
			- Exposure of coarse aggregates

Fig. 3 Schematic view of test setup and instrumentation according to EN 13230-2 (2016) ((CEN) 2009).

distance from the edge of each PSC tie to the point of loading was 545 mm. After the loading tests, the fractured pieces of PSC ties were collected for subsequent microstructural analyses. For the collected ties, three PSC ties were used for the loading test, except for the Map-cracked tie.

2.3 Sample Preparation for Microstructure Analyses

An optical microscope (Axio Zoom Microscope, Zeiss, Germany) was used to observe interfacial regions between aggregate and mortar matrix and identify reaction rims around aggregates. To this end, a sliced sample with a thickness of 5 mm was prepared using a precision saw to obtain cross-sections showing microstructures between cement paste and aggregate.

Coarse aggregates were separated using a steel brush from the collected PSC samples and then finely ground. After brushing, cement paste powders were also collected separately using sieves. The cement paste powders were then immersed in isopropanol and vacuum-dried for 2 days to prevent further hydration and carbonation.

Powder X-ray diffraction (XRD) patterns (D/MAX2500V/PC, Rigaku, Japan) were taken for the

ground aggregates and cement paste powders, respectively. The 2θ scanning range was 5–60° with an incident beam of Cu-Kα radiation ($\lambda = 1.5418$ Å). The measured XRD patterns were analyzed using the X'pert High-Score program (PANalytical 2012) with the Inorganic Crystal Structure Database (ICSD) (Allmann & Hinek, 2007) and the International Center for Diffraction Data (ICDD) PDF-2 database ("International centre for diffraction data (ICDD)" 2000).

Thermogravimetric (TG) analysis (Q500, TA Instruments, USA) was conducted for the cement paste powders in a nitrogen gas with an alumina pan and a heating rate of 30 °C/min from room temperature to 1000 °C (Jeon et al., 2018).

The inductively coupled plasma-optical emission spectroscopy (ICP-OES) tests were performed to examine the potential alkali-silica reactivity of the aggregates in the collected PSC ties by using a spectrometer (700-ES, Varian, USA). Then, 25 g of 0.15–0.30 mm sized aggregates were prepared and immersed in 25 mL of 1 N sodium hydroxide (NaOH) and saturated calcium hydroxide (Ca(OH)$_2$) solutions at 80 °C for 1, 2, and 7 days. At each day (i.e., at 1, 2, and 7 days), after filtering the samples, the liquid portions were tested to determine the concentrations of dissolved silicon (Si), aluminum (Al), sodium (Na), and potassium (K) using ICP-OES. The immersion period was 1, 2, and 7 days.

In addition, the petrographic examination was conducted using a polarized microscope (Leica DM4 P, Leica Microsystems, Germany); for the test, thin-sectioned (< 30 μm) aggregates were prepared. The test identified constituent minerals of the coarse aggregates in the PSC ties and compared the sizes of quartz grains among the samples.

Scanning electron microscopy (SEM) (Quanta200, FEI, USA) was employed to obtain secondary electron (SE) and backscattered electron (BSE) images of the sliced

Jeon *et al. Int J Concr Struct Mater*   (2022) 16:57

Page 5 of 15

concrete samples. The SEM specimens were immersed in isopropyl alcohol to carry out solvent exchange method for preserving the original microstructures of the concrete sample. For the SE images, the fractured samples were used without cutting or polishing to preserve the original condition of the specimen. For the BSE images, the PSC tie samples were sliced into 2 mm thicknesses with a precision saw and impregnated using epoxy resin. The impregnated samples were polished using an EcoMet 250 Grinder-Polisher (Buehler, USA).

3 Results and Discussion

3.1 Static Flexural Loading Test

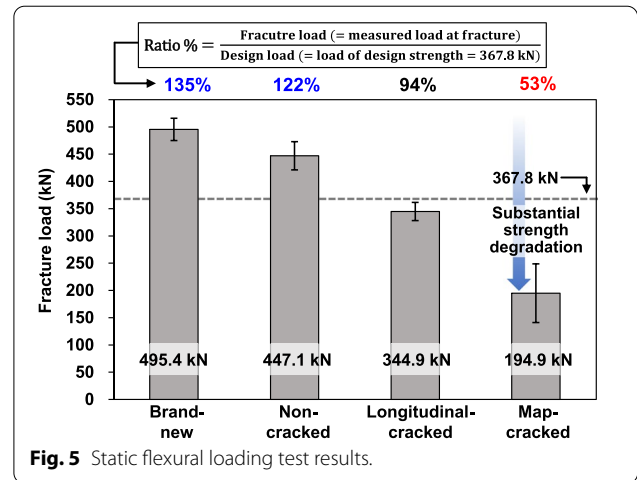The results of the static flexural loading test for the PSC ties are presented in Figs. 4 and 5. The fracture loads

$$\text{Ratio \%} = \frac{\text{Fracutre load (= measured load at fracture)}}{\text{Design load (= load of design strength = 367.8 kN)}}$$

Fig. 5 Static flexural loading test results.
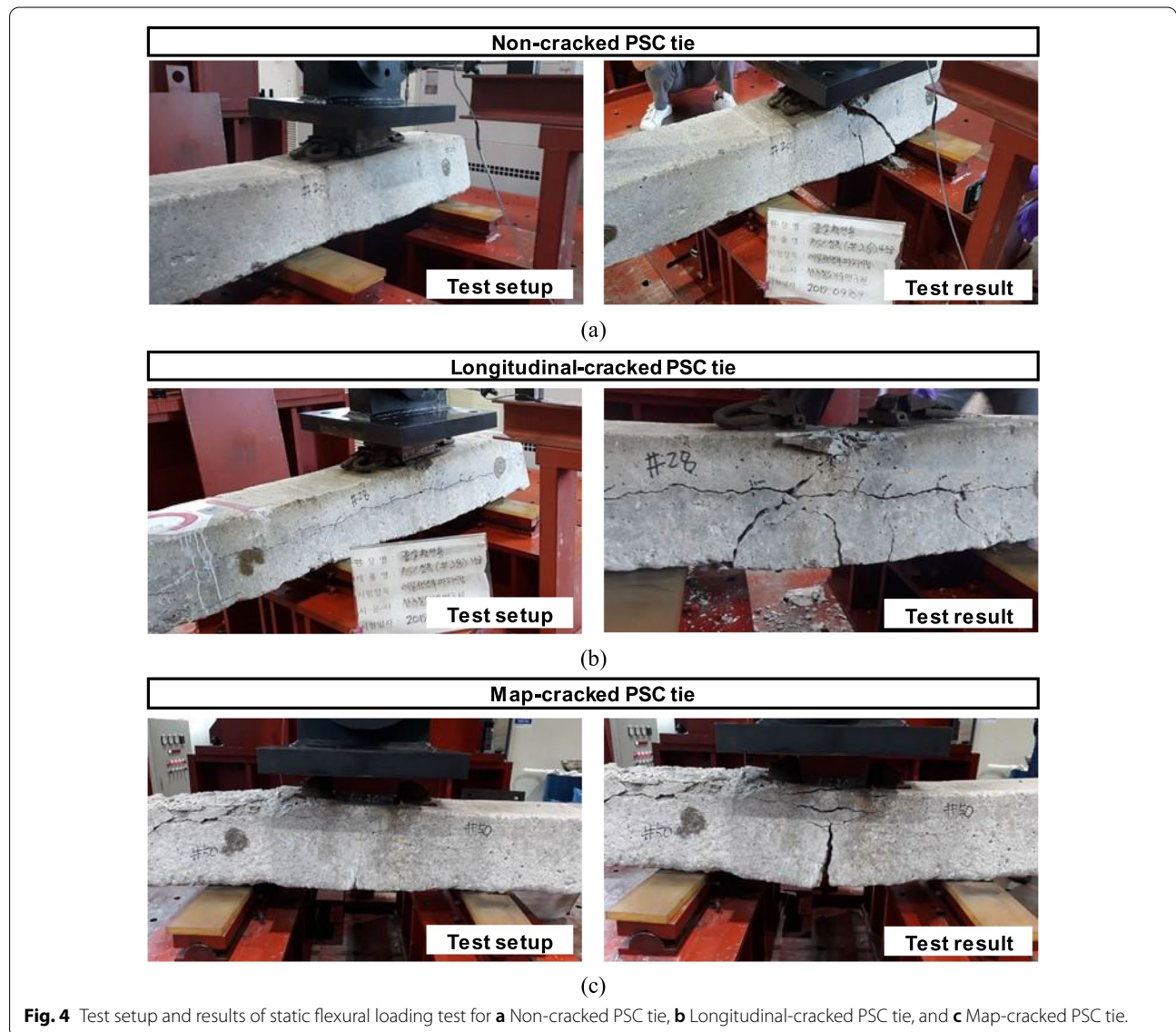
Fig. 4 Test setup and results of static flexural loading test for **a** Non-cracked PSC tie, **b** Longitudinal-cracked PSC tie, and **c** Map-cracked PSC tie.
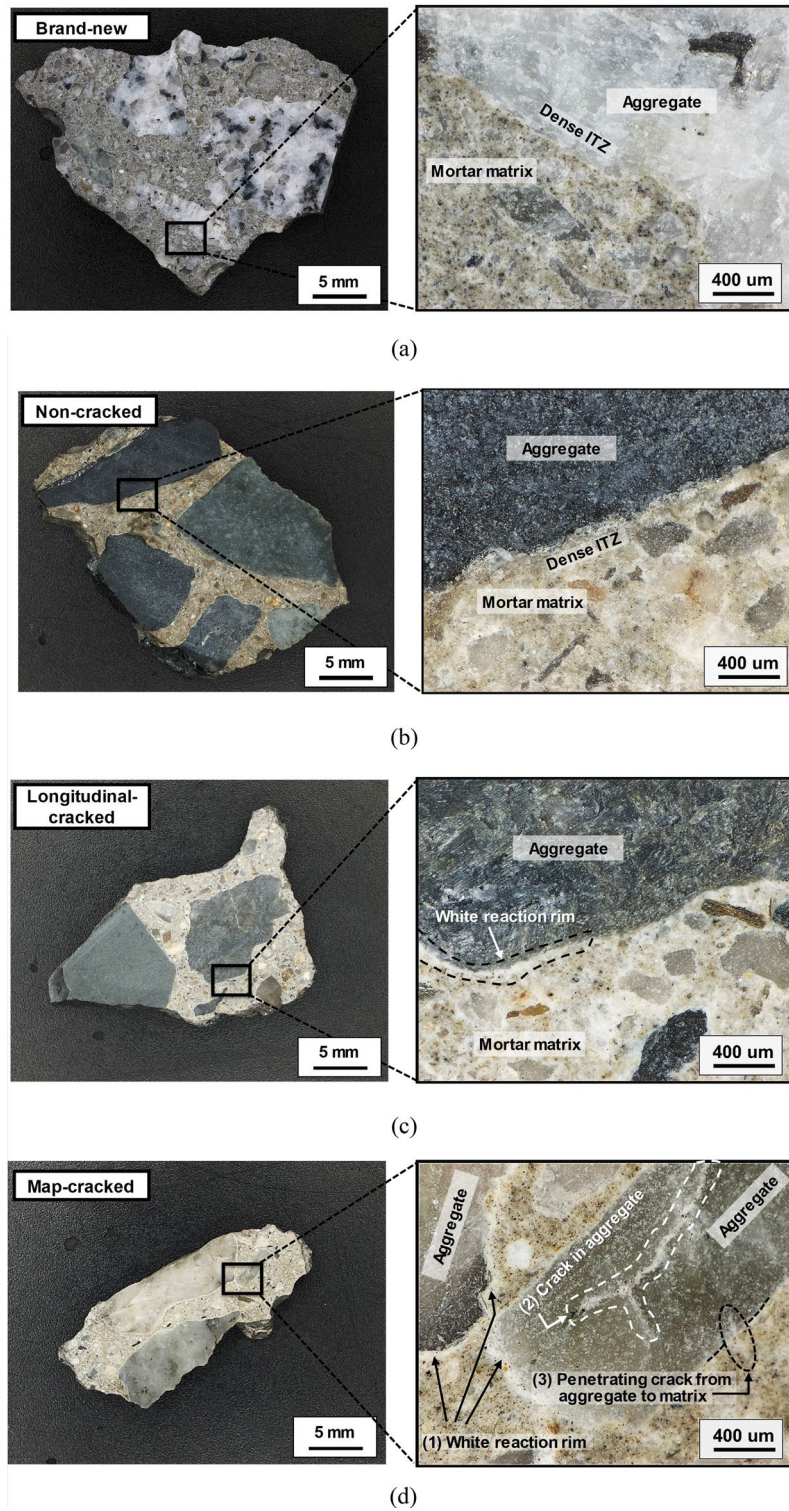
Fig. 6 Optical microscopic images of sliced concrete samples of **a** Brand-new, **b** Non-cracked, **c** Longitudinal-cracked, and **d** Map-cracked.
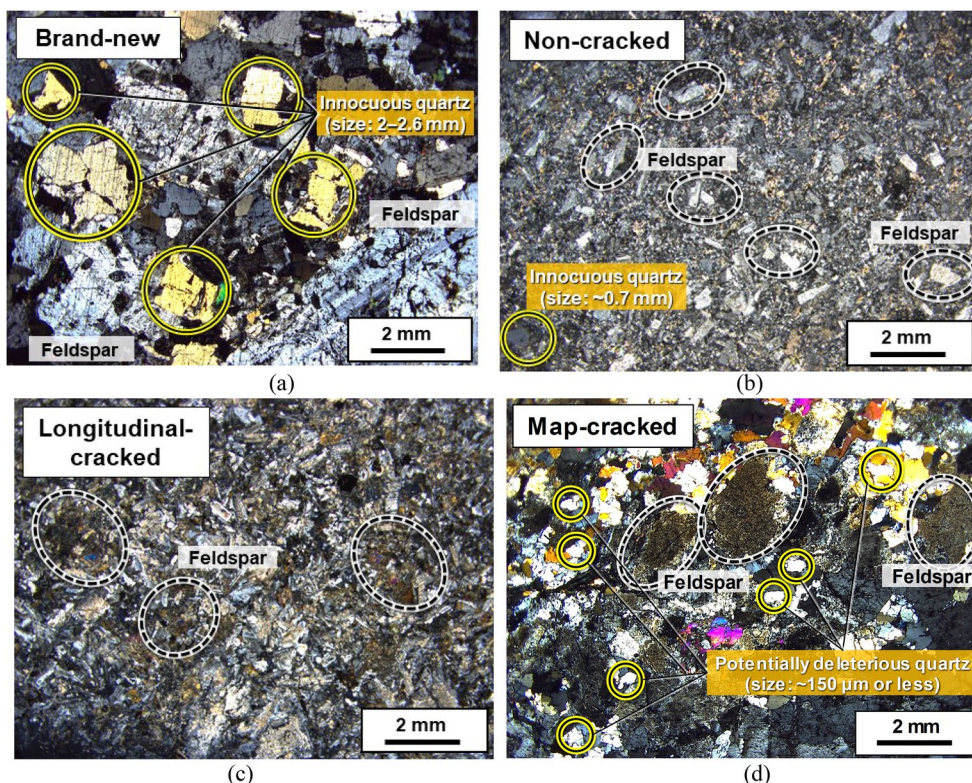
Fig. 7 Photographs taken by polarized light microscope of coarse aggregates from **a** Brand-new, **b** Non-cracked, **c** Longitudinal-cracked, and **d** Map-cracked. Quartz grains are highlighted by a solid line of circles, and feldspar grains are indicated by dashed ellipses.

of the Brand-new PSC ties ($=495.4$ kN) and the Non-cracked PSC ties ($=447.1$ kN) satisfied the design load ($=367.8$ kN), which is the design flexural strength of the PSC ties according to EN 13230-2 (2016) [9,13]. In Fig. 5, although the Longitudinal-cracked PSC ties showed a significantly lower fracture load ($=344.9$ kN) than those of Brand-new and Non-cracked PSC ties, the ties exhibited only a slightly lower fracture load than the design load despite the presence of visible cracks. However, the fracture load of the Map-cracked PSC ties ($=194.9$ kN) was only $\sim 53\%$ of the design load. Given that the strength degradation indicates the generation of significant damage inside the concrete, the Map-cracked PSC ties must be rejected for use; in addition, the Longitudinal-cracked PSC ties also should not be used unless proper maintenance is taken, as their strengths are expected to decrease over time.

3.2 Optical Microscopy

The optical microscopic images of the sliced PSC tie samples are depicted in Fig. 6. Each concrete sample contained coarse aggregates with different color tints and textures.

The Brand-new and Non-cracked samples demonstrated relatively dense interfacial transition zones (ITZ) and no visible cracks (see the magnified photographs in Fig. 6). However, white reaction rims were observed around coarse aggregates in the Longitudinal-cracked and Map-cracked samples. In particular, the Map-cracked sample exhibited three distinct features, as shown in Fig. 6d: (1) white reaction rims around aggregates, (2) internal cracks in aggregates, and (3) cracks penetrating from aggregate to the matrix.

Previous studies reported that deteriorations due to ASR and/or DEF were mainly evidenced by white reaction rims around aggregates by optical microscope (Rajabipour et al., 2015; Thomas et al., 2008); however, the internal cracks in aggregates and the cracks penetrating aggregates were only related to ASR damage (Rajabipour et al., 2015). Thus, the cracks (Fig. 2) and the strength degradations (Fig. 5) in the Longitudinal-cracked and Map-cracked ties might be related with the ASR and/or DEF. The detailed microstructural evidence of the deterioration will be discussed further in Sects. 3.3, 3.4, 3.5, 3.6, 3.7.
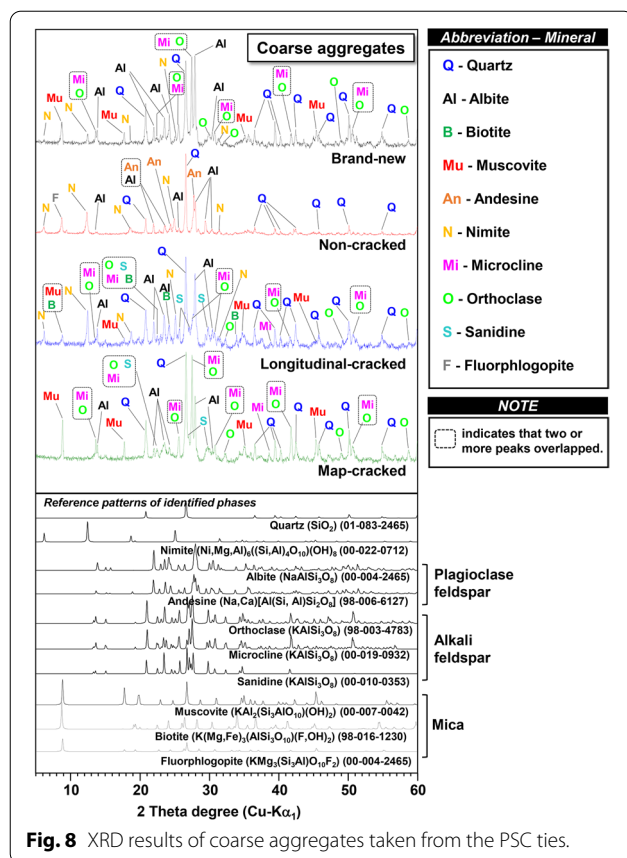
Jeon *et al. Int J Concr Struct Mater*   (2022) 16:57

Page 8 of 15

Fig. 8 XRD results of coarse aggregates taken from the PSC ties.

3.3 Petrographic Analysis

Fig. 7 shows the results of the polarizing microscope observation of coarse aggregates. Most mineral grains in the aggregates of all 15-year used PSC ties were severely damaged by long-term weathering. Quartz grains (see yellow circles in Fig. 7) were rarely observed in the polarized light microscope image because the crystal sizes of quartz in the sample were too small to be seen in the

microscope. Feldspar grains (see dotted ellipses in Fig. 7) were also observed.

Although crystalline quartz is significantly less alkalireactive than amorphous silica (SiO_2) in ASR, the reactivity of crystalline quartz can be increased by decreasing its crystal size; thus, microcrystalline (grain size $< \sim 130$ μm) and crypto-crystalline (grain size < 4 μm) quartz crystals possess a high alkali-silica reactivity (Sims & Nixon, 2003). In Brand-new and Non-cracked, the sizes of quartz grains were 2–2.6 mm and ~ 0.7 mm, respectively, and they were barely reactive (Alaejos & Lanza, 2012; Sims & Nixon, 2003) due to their large crystal sizes; however, in Map-cracked, the quartz sizes were approximately 150 μm or less (i.e., microcrystalline quartz), and thus the aggregates were potentially ASR reactive (Alaejos & Lanza, 2012; Sims & Nixon, 2003).
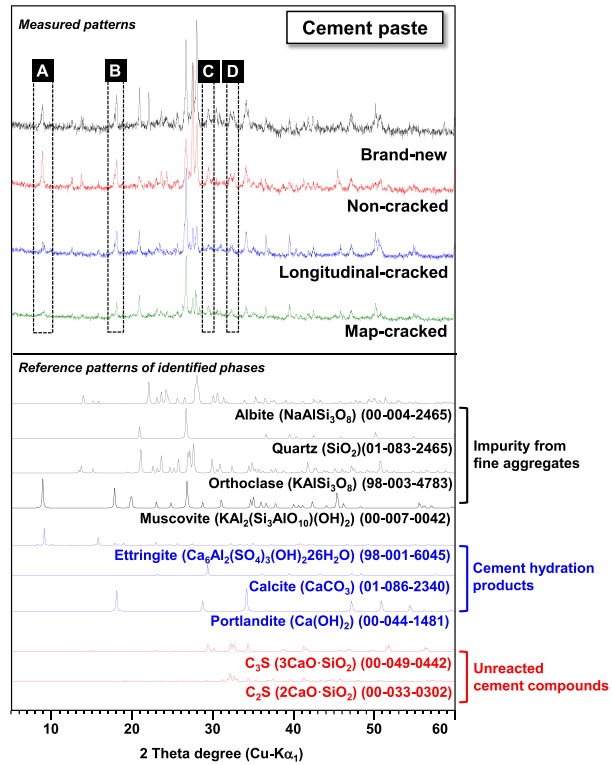
3.4 XRD

Fig. 8 shows the powder XRD patterns of coarse aggregates, which were taken from the PSC ties. The numbers in parentheses are the ICSD and ICDD reference numbers for the identified mineral phases. The minerals identified in the coarse aggregates from XRD are listed in Table 2. It is worth noting that none of the aggregates contained a hydrous form of silica (SiO_2) (e.g., opal, $SiO_2 \cdot nH_2O$), an amorphous form of silica (e.g., obsidian or volcanic glass), or other reactive components (e.g., chalcedony, tridymite, pyrex, and so on) which are well-known reactive and deleterious minerals causing ASR (Monteiro, 2006; Sims & Nixon, 2003).

In all coarse aggregates, both quartz (SiO_2) and albite ($NaAlSi_3O_8$) were identified, as shown in Fig. 8 and Table 2. Quartz is a mineral that generally constitutes concrete aggregates and is chemically and mechanically stable unless it is microcrystalline or highly strained (Monteiro, 2006; Sims & Nixon, 2003).
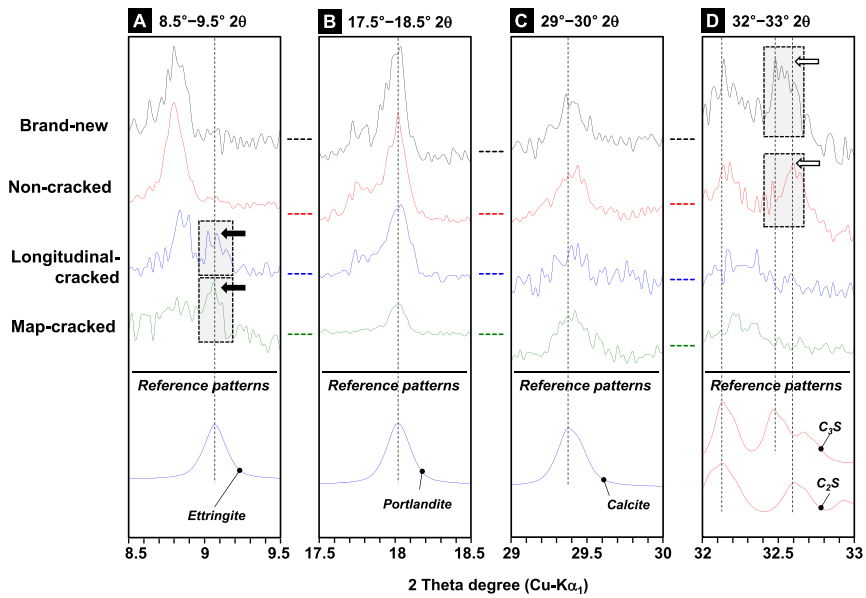
Table 2 Summary of minerals in the aggregates, identified from XRD.

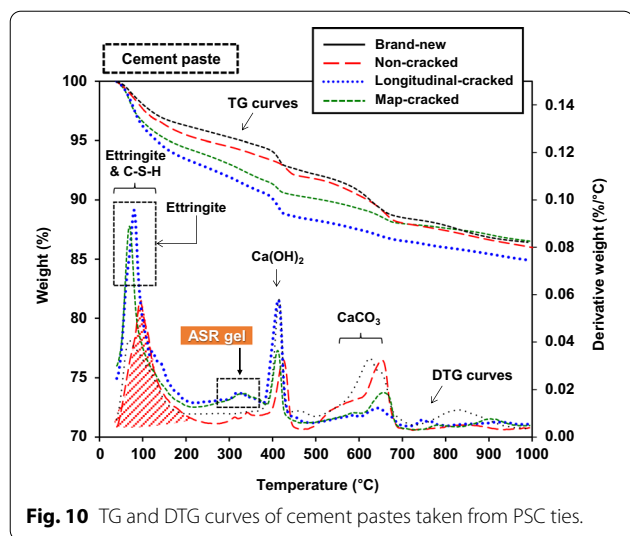|	Brand-new	Non-cracked	Longitudinal-cracked	Map-cracked	Note
Quartz	○○	○○	○○	○○	
Nimite	○○	○○	○○	–	
Albite	○○	○○	○○	○○	Plagioclase feldspar
Andesine	–	○○	–	–	Plagioclase feldspar
Orthoclase	○○	–	○	○○	Alkali feldspar
Microcline	○○	–	○	○○	Alkali feldspar
Sanidine	–	–	○○	○○	Alkali feldspar
Biotite	–	–	○○	–	Mica
Muscovite	○○	–	○	○○	Mica
Fluorphlogopite	–	○○	–	–	Mica

○○ present, ○ possibly present, and – not detected.

Fig. 9 XRD results of cement pastes taken from collected PSC ties: **a** full XRD results and identified phases, and **b** detailed magnified patterns for four 2θ ranges in **a**. Small amounts of aggregate minerals were still left in XRD after sample preparation.
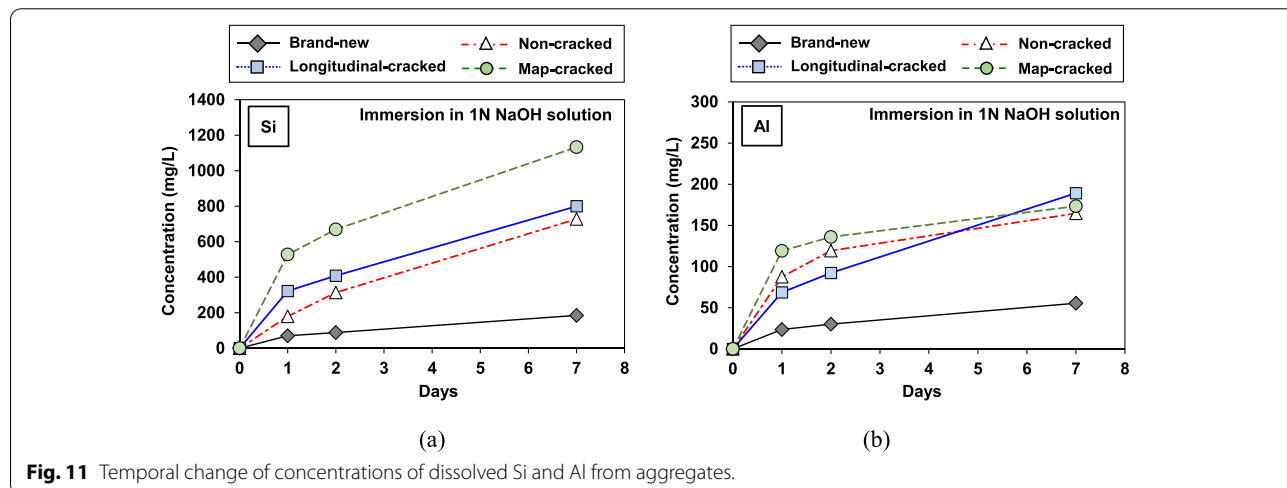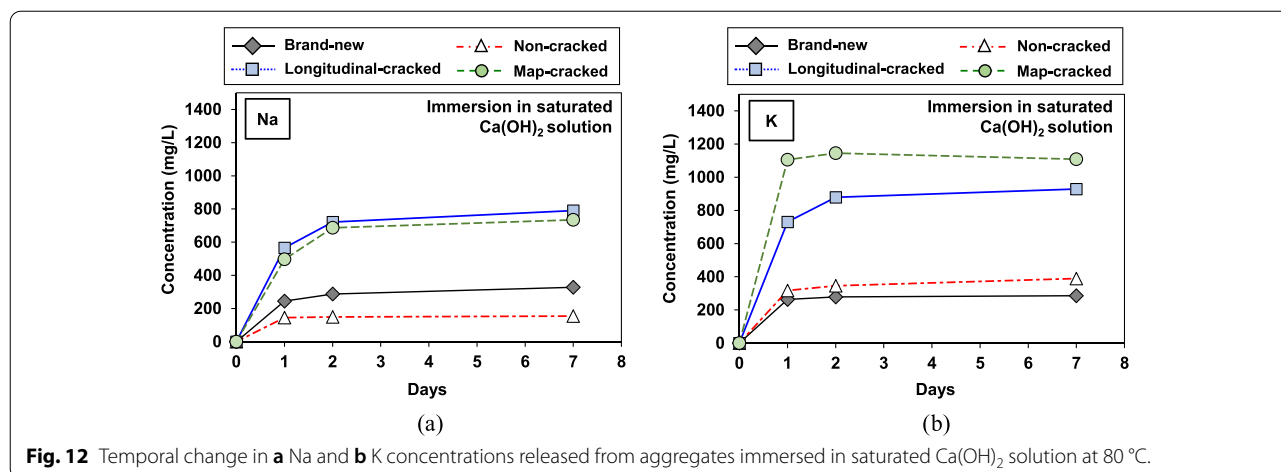
Fig. 10 TG and DTG curves of cement pastes taken from PSC ties.

of alkali-bearing aggregates into concrete pore solution, resulting in expansive ASR cracking even in low alkali cement concretes (Constantiner & Diamond, 2003; Locati et al., 2010). The influences of the alkali content in aggregates on the damage of PSC ties are discussed extensively in Sects. 3.6 to 3.7.

Biotite $(K(Mg,Fe)_3(AlSi_3O_{10})(F,OH)_2)$,   muscovite $(KAl_2Si_4O_{10}(OH)_2)$, and fluorphlogopite $(KMg_3(Si_3Al)O_{10}F_2)$ belong to the mica group (Grattan-Bellew & Beaudoin, 1980). Previous studies (Grattan-Bellew & Beaudoin, 1980; Tagnit-Hamou et al., 2005) reported that micas in concrete aggregates might cause concrete deterioration, as micas have a porous laminar structure that may provide a path for mobility of water, and thus micas might react with alkalis and form expansive hydration products. However, in this study, micas (i.e., biotite, muscovite, and fluorphlogopite) were also found in the Non-cracked as well as the Longitudinal-cracked and Map-cracked; accordingly, in this study, the presence of micas did not necessarily cause the deterioration of concrete, and thus additional factors should be considered, such as the presence of reactive silica and alkali content. The influence of micas on the deterioration of concrete is discussed in more detail in Sect. 3.7.

Fig. 9 shows the XRD patterns of the paste taken from each concrete sample. In all samples, quartz, albite, and orthoclase were found in common, which originated from the remaining fine aggregates because fine aggregates were not completely removed during sample preparation. However, the relatively strong diffraction intensity of the crystalline phases of the aggregates made the identification of cement hydration products and unreacted cement compounds rather difficult; thus, in Fig. 9b, the XRD patterns were further analyzed for hydration products using four specific 2θ ranges:

All coarse aggregates contained feldspar group minerals, such as albite $(NaAlSi_3O_8)$, microcline $(KAlSi_3O_8)$, sanidine $(KAlSi_3O_8)$, orthoclase $(KAlSi_3O_8)$, or andesine $((Na, Ca)Al(Si, Al)Si_2O_8)$. In this study, andesine was only found in the aggregates in the Non-cracked sample belonging to plagioclase feldspar minerals, which are solid solutions between albite and anorthite $(NaAlSi_3O_8–CaAl_2Si_2O_8)$ (Benisek et al., 2010; Locati et al., 2010). However, the aggregates in the Longitudinal-cracked and Map-cracked mostly contained orthoclase, microcline, and sanidine, which belong to alkali feldspar minerals that are solid solutions between K-feldspar and albite $(KAlSi_3O_8–NaAlSi_3O_8)$ (Benisek et al., 2010; Locati et al., 2010). It is worth noting that aggregates having alkalis may act as an alkali reservoir in concrete, given that previous studies have reported the possibility of alkali leaching from feldspar minerals or other types

Fig. 11 Temporal change of concentrations of dissolved Si and Al from aggregates.

Jeon *et al. Int J Concr Struct Mater*   (2022) 16:57

Page 11 of 15

Fig. 12 Temporal change in **a** Na and **b** K concentrations released from aggregates immersed in saturated Ca(OH)$_2$ solution at 80 ℃.

8.5°–9.5°, 17.5°–18.5°, 29°–30°, and 32°–33° (also see broken line boxes with A, B, C, and D, respectively, in Fig. 9a). Note that in 8.5°–9.5° 2θ, ettringite was only found in the Longitudinal-cracked and Map-cracked (see the arrows in A in Fig. 9b). The presence of ettringite could be an evidence of DEF (Hime, 1996; H F W Taylor et al., 2001). Ca(OH)$_2$ and calcite were identified in all samples. Unreacted cement compounds (i.e., C$_2$S (2CaO·SiO$_2$) and C$_3$S (3CaO·SiO$_2$)) were present in Brand-new and Non-cracked (see the white arrows in D in Fig. 9b). However, the cement compounds were barely identified in Longitudinal-cracked and Map-cracked; this observation may indicate that the hydration of these compounds increased due to water ingress from outside through the cracks.

3.5 TG Analysis

The TG and differential curves of TG (DTG) for cement pastes from the PSC ties are shown up to 1,000 ℃ in Fig. 10. Unlike XRD, TG/DTG cannot identify minerals in aggregates, such as albite, quartz, orthoclase, or muscovite, because these minerals are not thermally decomposed under 1000 ℃ (Lide, 2004). The large DTG peaks under 200 ℃ were due to dehydration of ettringite and C–S–H (Harry F W Taylor, 1997). Although it was difficult to precisely distinguish overlapped DTG peaks of C–S–H and ettringite (A Gruskovnjak et al., 2008; Astrid Gruskovnjak et al., 2011), the DTG peaks below 200 ℃ of the Brand-new and the Non-cracked samples were likely only attributable to the dehydration of C–S–H because ettringite was not detected in these samples in the XRD results (Fig. 9). The 15-year used PSC ties (i.e., Non-cracked, Longitudinal-cracked, and Map-cracked) showed significantly larger C–S–H peaks than that of the Brand-new PSC tie, possibly due to the longer hydration ages (i.e., ∼ 17 years vs. ∼ 1 year), resulting in more

formation of C–S–H. The DTG peaks below 200 ℃ of Longitudinal-cracked and Map-cracked samples were slightly more extensive than that of the Non-cracked sample (red-shaded area), probably due to the presence of ettringite and more hydration of cement compounds.

It is worth noting that the small DTG peaks around 350 ℃ were only found in Longitudinal-cracked and Map-cracked (see the dotted box in Fig. 10). The previous study reported that these DTG peaks were produced from the decomposition of ASR gel (Shi et al., 2019). Therefore, from the XRD and TG results, the deteriorations of the Longitudinal-cracked and Map-cracked PSC ties were likely related to ASR and DEF together. The large peaks around 410 ℃ were due to dehydration of Ca(OH)$_2$ (A Gruskovnjak et al., 2008). The DTG peaks at 600–700 ℃ and at 800–900 ℃ were attributed to the decomposition of calcite (Gabrovšek et al., 2006; Wang et al., 2004).

3.6 ICP-OES Analysis

Fig. 11 shows temporal change of concentrations of released Si and Al from aggregates in 1 N NaOH solution at 80 ℃. The magnitude of Si concentration was found from most significant to smallest in the following sample order: Map-cracked > Longitudinal-cracked > Non-cracked > Brand-new. The result indicates that the aggregates of more damaged ties had a more dissolvable (or reactive) state of Si than those of the less damaged ties. Although the concentration of Al did not follow the apparent trend of Si concentration, the aggregates in the damaged ties tended to release more Al. Thus, Fig. 11 demonstrates that the aggregates in Map-cracked PSC ties were the greatest in terms of chemical reactivity, and this was likely attributable to the presence of microcrystalline quartz, as discussed in Sect. 3.3. Although there were no well-known reactive siliceous minerals, such
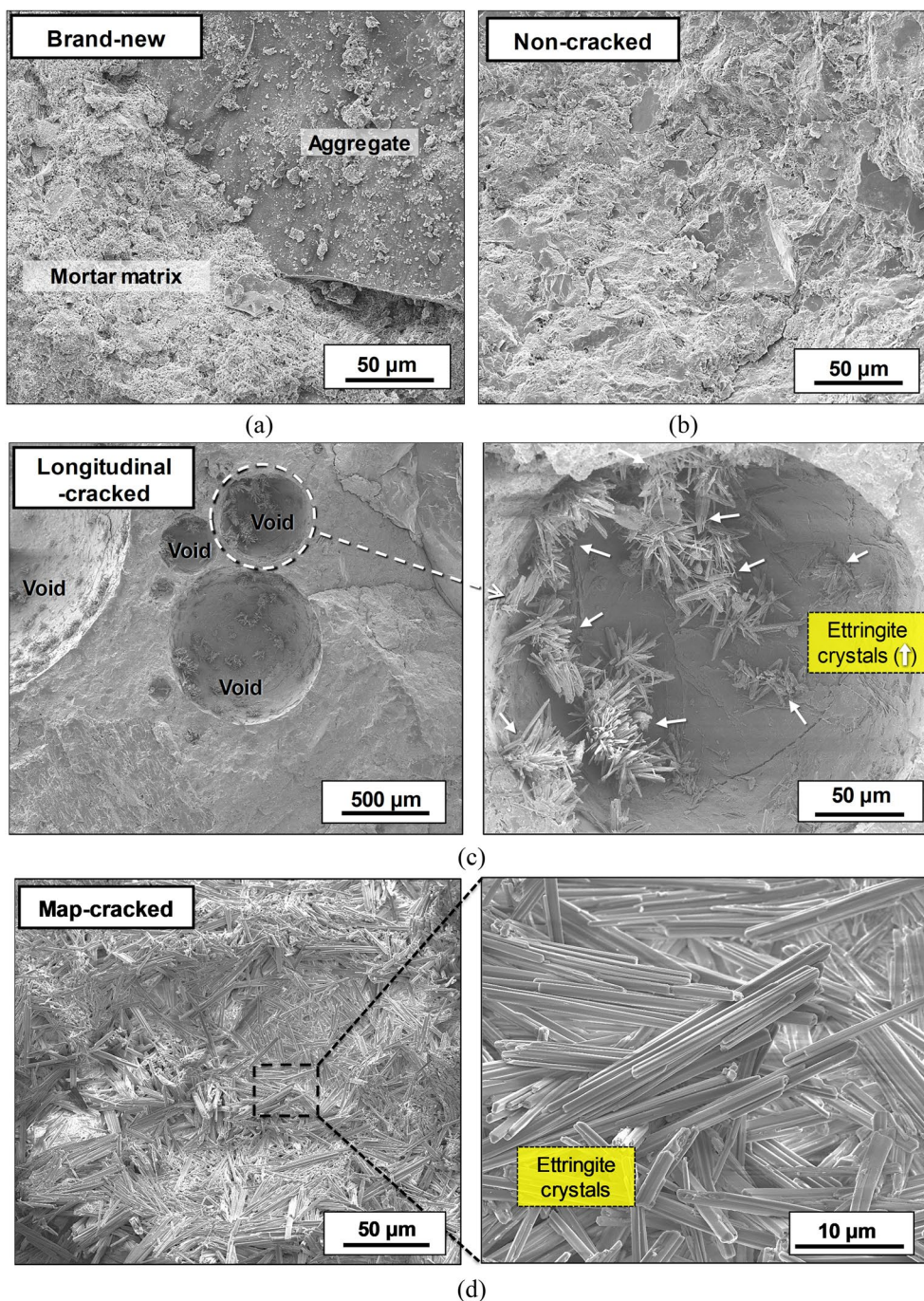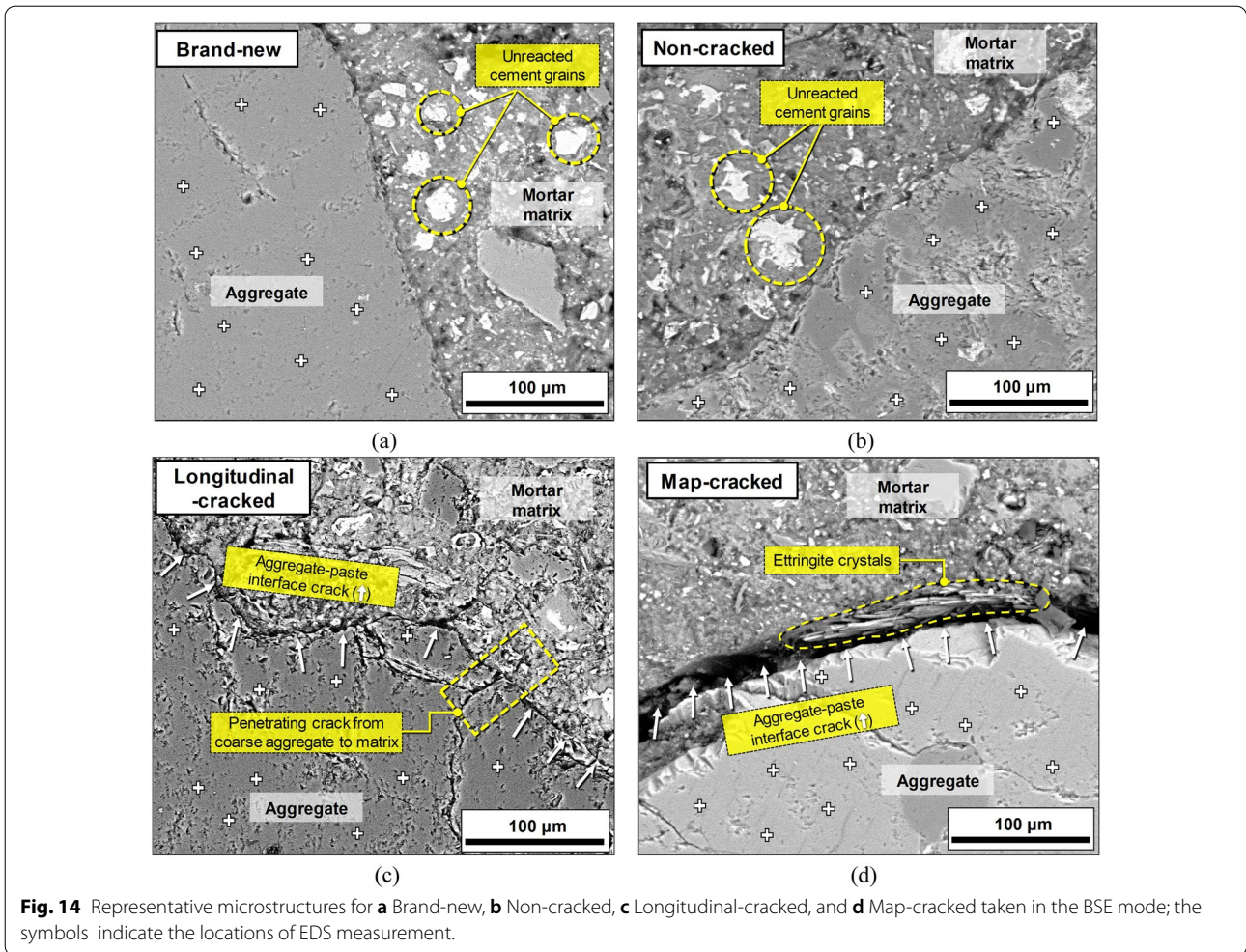
Fig. 13 Representative microstructures of fractured surfaces for **a** Brand-new, **b** Non-cracked, **c** Longitudinal-cracked, and **d** Map-cracked in SEM SE images.

as opal or obsidian, in aggregates for ASR in this study, microcrystalline quartz in aggregates likely played a role in supplying reactive SiO_2 to trigger ASR.

Fig. 12 shows the measured concentrations of alkalis (Na and K) with time from aggregates in saturated $Ca(OH)_2$ solution at 80 °C. In the results, Na and K ions were considerably more dissolved from the aggregates of Longitudinal-cracked and Map-cracked than those of Brand-new and Non-cracked. These dissolved alkali ions likely reacted with dissolved Si, resulting in the formation of an ASR gel. The alkali-bearing minerals in aggregates likely supplied enough alkalis for ASR.

Fig. 14 Representative microstructures for **a** Brand-new, **b** Non-cracked, **c** Longitudinal-cracked, and **d** Map-cracked taken in the BSE mode; the symbols indicate the locations of EDS measurement.

Fig. 15 Ternary diagram of aggregates' elemental compositions (Si–Al-alkalis) constructed using the EDS results of aggregates.

3.7 SEM Analysis

Fig. 13 shows the SEM SE images of fractured surfaces of the PSC tie samples. Unlike Brand-new and Non-cracked, the Longitudinal-cracked and Map-cracked samples show ettringite crystals in voids. In particular, massive crystals of ettringite were only found in interface of paste and aggregate in Map-cracked, as shown in Fig. 13d. However, it was not found in the surface of Longitudinal-cracked sample. The presence of massive ettringite crystals is the typical microstructural feature of DEF, as the recrystallization of ettringite produces expansive pressure in hardened concrete, resulting in cracks and strength degradation (H F W Taylor et al., 2001).

The BSE images for polished concrete samples are provided in Fig. 14. The ITZs were densely filled in Brand-new and Non-cracked, while cracks were present in the ITZs in Longitudinal-cracked and Map-cracked (white arrows in Fig. 14c and d). In Brand-new and Non-cracked, many unreacted cement compound grains (Scrivener, 2004) were present, unlike

Jeon *et al. Int J Concr Struct Mater*   (2022) 16:57

Page 14 of 15
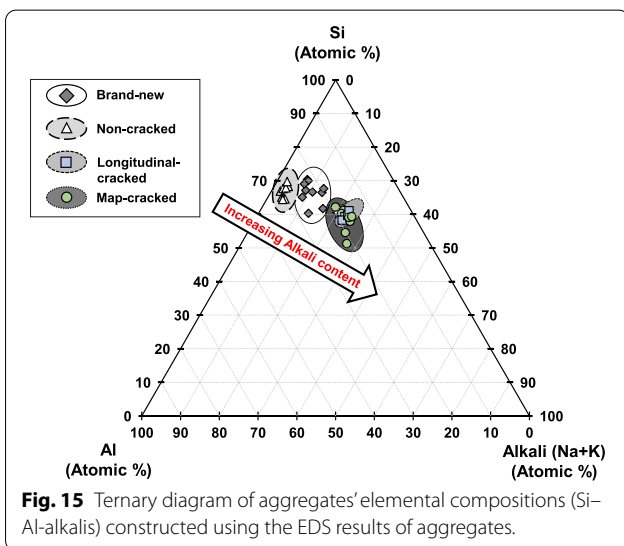
Longitudinal-cracked and Map-cracked, as stated in the XRD result (Fig. 9). In Longitudinal-cracked, a penetrating crack from aggregate into matrix was also observed, and, in Map-cracked, ettringite crystals were detected in the crack of the aggregate–paste interface.

Fig. 15 shows the ternary diagram of Si, Al, and alkalis (Na, K) elemental compositions constructed using the EDS results in Fig. 14. In this study, alkali contents in aggregates were calculated from the most significant to the smallest in the following sample order: Map-cracked ≈ Longitudinal-cracked > Brand-new > Non-cracked, and the alkali content in aggregates was associated with the deterioration of the PSC ties because the samples with aggregates having high alkali contents tended to have severe deterioration. Therefore, in this study, the alkali-bearing minerals (i.e., alkali feldspars in Fig. 8) were most likely the alkali supply for ASR. Besides, mica in aggregates could promote ASR due to its porous structure, which helps in easy ingress of water (Grattan-Bellew & Beaudoin, 1980; Tagnit-Hamou et al., 2005).

4 Conclusions

This study investigates the deteriorations of the 15-year used PSC ties utilized in Korea. Using the field inspection, static flexural loading test, optical microscope, XRD, TG/DTG, ICP-OES, polarization microscope analysis, and SEM with EDS, the following conclusions are made:

(1) In some of the collected dismantled PSC ties, not only longitudinal cracks on sides but also map cracks on surfaces were observed. The strength of the PSC ties with cracks (i.e., Longitudinal-cracked and Map-cracked) did not satisfy the design flexural strength specified from EN 13,230–2 (2016). In particular, the Map-cracked PSC ties exhibited substantial strength degradation to the extent that use must be rejected.

(2) The deteriorations were likely related to ASR and DEF together, as the presence of massive ettringite crystals and the decomposition of ASR gel was found from the XRD, TG, and SEM results. In the PSC ties with cracks, white reaction rims around aggregates were observed, which is optical microscopic evidence of deteriorations by ASR and/or DEF; furthermore, massive crystals of ettringite at interface between aggregate and paste were also found, which is a typical microstructural feature of DEF.

(3) The aggregates in the PSC ties with cracks were potentially reactive aggregates, and its high alkali-silica reactivity was likely attributable to the presence of microcrystalline quartz. They likely sup-

plied reactive SiO_2 to trigger ASR. Furthermore, the curing temperature during manufacture of the PSC ties might also contribute to the deterioration.

(4) The alkali content in aggregates was associated with the deterioration of the PSC ties. Although it is unclear whether alkalis in Portland cement may have contributed to the ASR of the PSC ties in this study, the alkali-bearing minerals (i.e., alkali feldspars) in aggregates likely supplied enough alkalis for ASR. The dissolved alkali ions likely reacted with dissolved Si, resulting in the formation of an ASR gel. Moreover, mica in aggregates could promote ASR due to its porous structure, which contributes to easy ingress of water.

Author contributions
DJ: conceptualization, methodology, investigation, formal analysis, writing—original draft preparation, writing—review and editing; JY: investigation, formal analysis; JK: resources, project administration; SY: writing—review and editing; YB: writing—review and editing, resources, supervision, funding acquisition, project administration; JEO: writing—review and editing, resources, supervision, project administration. All authors read and approved the final manuscript.

Authors' information
Dongho Jeon is a Postdoctoral Researcher in Department of Civil and Environmental Engineering at Seoul National University, Seoul, Korea and was in Department of Urban and Environmental Engineering at Ulsan National Institute of Sciences and Technology (UNIST), Ulsan, Korea.
Juan Yu is a Graduate Student in Department of Urban and Environmental Engineering at Ulsan National Institute of Sciences and Technology (UNIST), Ulsan, Korea.
Jihwan Kim is a Senior Researcher in High-Speed Railroad Systems Research Center at Korea Railroad Research Institute, Korea.
Seyoon Yoon is an Associate Professor in Major of Civil Engineering at Kyonggi University, Suwon-Si, Korea.
Younghoon Bae is a Principal Researcher in High-Speed Railroad Systems Research Center at Korea Railroad Research Institute, Korea.
Jae Eun Oh is a Full Professor in Department of Urban and Environmental Engineering at Ulsan National Institute of Sciences and Technology (UNIST), Ulsan, Korea.

Declarations

Jeon *et al. Int J Concr Struct Mater*   *(2022) 16:57*

Page 15 of 15

References

Alaejos, P., & Lanza, V. (2012). Influence of equivalent reactive quartz content on expansion due to alkali silica reaction. *Cement and Concrete Research, 42*(1), 99–104. https://doi.org/10.1016/j.cemconres.2011.08.006

Allmann, R., & Hinek, R. (2007). The introduction of structure types into the Inorganic Crystal Structure Database ICSD. *Acta Crystallographica Section a: Foundations of Crystallography, 63*(5), 412–417. https://doi.org/10.1107/S0108767307038081

Bae, Y., Bae, J. H., Kim, M. C., & Jang, S. Y. (2018). Flexural Strength of cracked prestressed concrete sleepers used on Gyeongbu high speed line. *Journal of the Korean Society for Railway, 21*(9), 900–915. https://doi.org/10.7782/JKSR.2018.21.9.900

Benisek, A., Dachs, E., & Kroll, H. (2010). A ternary feldspar-mixing model based on calorimetric data: Development and application. *Contributions to Mineralogy and Petrology, 160*(3), 327–337. https://doi.org/10.1007/s00410-009-0480-8

(CEN), E. C. for S. (2009). Railway applications-track-concrete sleepers and bearers part 2: Prestressed monoblock sleepers.

Constantiner, D., & Diamond, S. (2003). Alkali release from feldspars into pore solutions. *Cement and Concrete Research, 33*(4), 549–554. https://doi.org/10.1016/S0008-8846(02)01001-3

Gabrovšek, R., Vuk, T., & Kaučič, V. (2006). Evaluation of the hydration of Portland cement containing various carbonates by means of thermal analysis. *Acta Chimica Slovenica, 53*, 159–165.

Grattan-Bellew, P. E., & Beaudoin, J. J. (1980). Effect of phlogopite mica on alkali-aggregate expansion in concrete. *Cement and Concrete Research, 10*(6), 789–797. https://doi.org/10.1016/0008-8846(80)90007-1

Gruskovnjak, A., Lothenbach, B., Winnefeld, F., Figi, R., Ko, S.-C., Adler, M., & Mäder, U. (2008). Hydration mechanisms of super sulphated slag cement. *Cement and Concrete Research, 38*(7), 983–992. https://doi.org/10.1016/j.cemconres.2008.03.004

Gruskovnjak, A., Lothenbach, B., Winnefeld, F., Münch, B., Figi, R., Ko, S.-C., et al. (2011). Quantification of hydration phases in supersulfated cements: Review and new approaches. *Advances in Cement Research, 23*(6), 265–275. https://doi.org/10.1680/adcr.2011.23.6.265

Hime, W. G. (1996). Delayed ettringite formation-A concern for precast concrete? *PCI Journal, 41*(4), 26–30. https://doi.org/10.15554/pcij.07011996.26.30

Ho, D. W. S., Chua, C. W., & Tam, C. T. (2003). Steam-cured concrete incorporating mineral admixtures. *Cement and Concrete Research, 33*(4), 595–601. https://doi.org/10.1016/S0008-8846(02)01028-1

International centre for diffraction data (ICDD). (2000). *Swarthmore, Pa, 19081*.

International Union of Railways. (2004). *Design of monoblock concrete sleepers*. International Union of Railways.

Jeon, D., Yum, W. S., Jeong, Y., & Oh, J. E. (2018). Properties of quicklime(CaO)-activated Class F fly ash with the use of CaCl2. *Cement and Concrete Research, 111*(May), 147–156. https://doi.org/10.1016/j.cemconres.2018.05.019

Jeong, Y., Park, H., Jun, Y., Jeong, J. H., & Oh, J. E. (2015). Microstructural verification of the strength performance of ternary blended cement systems with high volumes of fly ash and GGBFS. *Construction and Building Materials, 95*, 96–107. https://doi.org/10.1016/j.conbuildmat.2015.07.158

Kaewunruen, S., & Remennikov, A. M. (2006). Sensitivity analysis of free vibration characteristics of an in situ railway concrete sleeper to variations of rail pad parameters. *Journal of Sound and Vibration, 298*(1–2), 453–461. https://doi.org/10.1016/j.jsv.2006.05.034

Koh, T., & Hwang, S. (2015). Field evaluation and durability analysis of an eco-friendly prestressed concrete sleeper. *Journal of Materials in Civil Engineering, 27*(7), B4014009. https://doi.org/10.1061/(ASCE)MT.1943-5533.0001109

Lide, D. R. (2004). *CRC handbook of chemistry and physics* (Vol. 85). CRC Press.

Locati, F., Marfil, S., Baldo, E., & Maiza, P. (2010). Na2O, K2O, SiO2 and Al2O3 release from potassic and calcic–sodic feldspars into alkaline solutions. *Cement and Concrete Research, 40*(8), 1189–1196. https://doi.org/10.1016/j.cemconres.2010.04.005

Ma, K., Long, G., & Xie, Y. (2017). A real case of steam-cured concrete track slab premature deterioration due to ASR and DEF. *Case Studies in Construction Materials, 6*, 63–71. https://doi.org/10.1016/j.cscm.2016.12.001

Monteiro, P. (2006). *Concrete: microstructure, properties, and materials*. McGraw-Hill Publishing.

PANalytical, B. (2012). 'Pert HighScore Plus software, version 3.0 e. Almelo.

Rajabipour, F., Giannini, E., Dunant, C., Ideker, J. H., & Thomas, M. D. A. (2015). Alkali–silica reaction: Current understanding of the reaction mechanisms and the knowledge gaps. *Cement and Concrete Research, 76*, 130–146. https://doi.org/10.1016/j.cemconres.2015.05.024

Remennikov, A. M., & Kaewunruen, S. (2014). Experimental load rating of aged railway concrete sleepers. *Engineering Structures, 76*, 147–162. https://doi.org/10.1016/j.engstruct.2014.06.032

Sahu, S., & Thaulow, N. (2004). Delayed ettringite formation in Swedish concrete railroad ties. *Cement and Concrete Research, 34*(9), 1675–1681. https://doi.org/10.1016/j.cemconres.2004.01.027

Scrivener, K. L. (2004). Backscattered electron imaging of cementitious microstructures: Understanding and quantification. *Cement and Concrete Composites, 26*(8), 935–945. https://doi.org/10.1016/j.cemconcomp.2004.02.029

Shi, Z., Geng, G., Leemann, A., & Lothenbach, B. (2019). Synthesis, characterization, and water uptake property of alkali-silica reaction products. *Cement and Concrete Research, 121*, 58–71. https://doi.org/10.1016/j.cemconres.2019.04.009

Sims, I., & Nixon, P. (2003). RILEM recommended test method AAR-1: Detection of potential alkali-reactivity of aggregates—petrographic method. *Materials and Structures, 36*(7), 480–496. https://doi.org/10.1007/BF02481528

Tagnit-Hamou, A., Saric-Coric, M., & Rivard, P. (2005). Internal deterioration of concrete by the oxidation of pyrrhotitic aggregates. *Cement and Concrete Research, 35*(1), 99–107. https://doi.org/10.1016/j.cemconres.2004.06.030

Taylor, H. F. W. (1997). *Cement chemistry* (Vol. 2). Thomas Telford London.

Taylor, H. F. W., Famy, C., & Scrivener, K. L. (2001). Delayed ettringite formation. *Cement and Concrete Research, 31*(5), 683–693. https://doi.org/10.1016/S0008-8846(01)00466-5

Thomas, M., Folliard, K., Drimalas, T., & Ramlochan, T. (2008). Diagnosing delayed ettringite formation in concrete structures. *Cement and Concrete Research, 38*(6), 841–847. https://doi.org/10.1016/j.cemconres.2008.01.003

Thun, H., Utsi, S., & Elfgren, L. (2008). Load carrying capacity of cracked concrete railway sleepers. *Structural Concrete, 9*(3), 153–161. https://doi.org/10.1680/stco.2007.00024

Wang, K., Shah, S. P., & Mishulovich, A. (2004). Effects of curing temperature and NaOH addition on hydration and strength development of clinker-free CKD-fly ash binders. *Cement and Concrete Research, 34*(2), 299–309. https://doi.org/10.1016/j.cemconres.2003.08.003

Publisher's Note

Springer Nature remains neutral with regard to jurisdictional claims in published maps and institutional affiliations.